Laser induced nanostructuration of vertically aligned carbon nanotubes coated with nickel oxide nanoparticles

A. Pérez del Pino[1,*], E. Gyorgy[1,2], S. Hussain[3], J. L. Andújar[3], E. Pascual[3], R. Amade[3], E. Bertrán[3]

[1]Instituto de Ciencia de Materiales de Barcelona, Consejo Superior de Investigaciones Científicas (ICMAB-CSIC), Campus UAB, 08193 Bellaterra, Spain

[2]National Institute for Lasers, Plasma and Radiation Physics, P. O. Box MG 36, 77125 Bucharest, Romania

[3]Departament de Física Aplicada, Universitat de Barcelona, C/Martí i Franqués 1, 08028 Barcelona, Spain

Abstract

A versatile method is explored to decorate vertically aligned multi-walled carbon nanotubes (VACNTs) with NiO nanostructures. Multi-walled VACNTs are grown by plasma enhanced chemical vapor deposition and coated with NiO nanoparticles (NPs) by drop casting. After that, the system is submitted to nanosecond pulsed UV laser irradiation in atmospheric environment. Laser irradiation provokes rapid heating-melting-cooling processes which lead to the recrystallization of NiO NPs on the outer walls of VACNTs. In this way, and depending on the laser fluence and the number of accumulated pulses, different nano-architectures such as continuous NiO coatings and spiny features on VACNTs are obtained. High resolution scanning and transmission electron microscopies and Raman spectroscopy, corroborated with photothermal simulations, suggest that the grown nanostructures are mainly created by the laser-induced high temperatures (photothermal mechanisms). However, the observed reconstruction of the outer graphitic shells of VACNTs point to the catalytic action of NiO NPs, probably induced by the direct action of the laser radiation.

Corresponding author. Tel: +34 935801853. E-mail: aperez@icmab.es (Angel Perez)

Keywords: vertically aligned carbon nanotubes, nickel oxide, carbon nanocomposites, laser nanostructuration

1. Introduction

For many electrical and electrochemical applications, conductive materials with an extended chemically active surface are required to improve the performance of the devices. Low dimensional sp^2-hybridized carbon nanostructures as carbon nanotubes (CNTs) and graphene-based materials are promising materials for this subject. Particularly, vertically aligned CNTs (VACNTs) can exhibit high electrical conductivity and adhesion to the substrate, in addition to large stability, mechanical flexibility and very large surface area able to interact with external molecules. Of particular importance for electronic devices is the low electric resistance in VACNT systems. VACNTs exhibit better electrical connection to the electrode and larger effective surface area for electrochemical applications than randomly, or horizontally aligned CNT yarns. Consequently, intense research efforts are being devoted to achieve controlled synthesis of these types of nanostructures, with the objective to develop high performance devices. For instance, VACNT forests have been synthesized for the fabrication of flexible supercapacitors with enhanced electric capacitance [1,2]. Besides, VACNTs with controlled structure have been also used as light-weight high specific surface current collector material for lithium batteries and IR radiation detectors [3-5]. Furthermore, and due to their large electrochemical active surface area, VACNTs have been also integrated in highly sensitive chemical sensors [6-8].

On the other hand, transition-metal oxides (TMO) have been also extensively studied in many application fields as supercapacitors, batteries and electrocatalysts for oxygen reduction reactions [9-12]. NiO appears as one of the most promising TMO material due to its nontoxicity, high chemical stability and good performance in faradaic reactions. However, TMO materials exhibit limited conductivity that precludes their practical application in electrochemical devices. In recent years, it has been demonstrated that the decoration of CNTs with TMO can increase their electrochemical performance [13-15]. In particular, NiO-CNT architectures have been reported to be good candidates for the fabrication of efficient electrochemical devices. Thus, NiO-CNT composites have been used to develop H_2 and volatile organic gas sensors [16,17]

as well as glucose sensors [18], high performance supercapacitors [19-21] and lithium-ion batteries [22-24]. Regarding catalytic applications, NiO-CNT materials have been used as electrocatalyst for water splitting and in microbial fuel cells [25,26]. These composites also show high catalytic performance for the oxidation removal of toluene and the electrochemical reduction of CO_2 [27,28].

Though the synthesis of NiO-CNT compounds by chemical and electrochemical methods are being developed, inherent limitations due to hydrophobic properties of CNTs, chemical incompatibilities of reagents or electro-induced damaging are still issues yet to be resolved in order to produce NiO-decorated CNT-based structures with improved performance for practical applications. Therefore, the design of new architectures by using innovative methodologies will play a vital role in achieving of materials with enhanced functionality. Laser processing techniques are an interesting alternative to conventional synthesis methods. It is widely reported that laser radiation can induce physical and chemical mechanisms in materials, usually coupled between them and far from the thermodynamic equilibrium, provoking phase transitions not achievable with conventional methods. For instance, significant diffusion and even selective melting processes can be induced in nanostructures due to the short and intense laser-induced thermal cycles [29,30]. Moreover, thin films composed of graphene oxide (GO) and GO decorated with TMO NPs have been recently reported to suffer complex structural transformations after their irradiation with nanosecond laser pulses [31-33]. Nonetheless, a scarce number of works reports structural transformations of carbon nanotubes by the action of laser irradiation [34-36] and, to our best knowledge, no works have been published regarding the laser irradiation of CNT-TMO hybrid nanomaterials.

Herein we study the effects of ultraviolet (UV) nanosecond pulsed laser irradiation in VACNT films coated with NiO NPs. The irradiations are conducted in air, at atmospheric pressure by accumulating a number of laser pulses at different laser fluences. Structural-compositional analyses reveal notable modification of the NiO/VACNT structure, led by thermally-activated diffusion-melting-recrystallization processes.

2. Materials and methods

Fig. 1 shows a scheme of the experimental procedure, composed of three steps. First of all, VACNTs were grown by means of plasma enhanced chemical vapor deposition technique (PECVD) (step "i" in Fig. 1). After that, NiO NPs were deposited on the VACNT layer (step "ii" in Fig. 1). Finally, the NiO/VACNT systems were irradiated with laser for achieving their recrystallization (step "iii" in Fig. 1). (i) A mat of carbon nanotubes was grown on boron doped p-Si wafers, 2" diameter, with low resistivity (range 0.01 0.02 Ω·cm). As usual, before each growing process, the pressure of the reactor was lowered below 4×10^{-4} Pa as a guaranty of clean conditions. Then, Ar gas was injected up to a pressure of 2 Pa. Silicon wafer was coated with 3 nm layer of Fe catalyst by magnetron sputtering, being the 3" Fe target excited at 50 W by RF power (13.56 MHz). PECVD was preferred as the simplest process to grow vertically aligned CNTs. In order to avoid oxidation of deposited materials, a mobile substrate holder allowed us performing a sequential processing of sputtering and PECVD inside the chamber without breaking the vacuum conditions [37]. For the present study, the PECVD synthesis of VACNTs was carried out heating at 680°C during 900 s in an atmosphere of NH_3/C_2H_2 gas mixture, where NH_3 was the carrier gas and C_2H_2 the precursor gas (Table 1). (ii) Dilute dispersions of NiO NPs (ca. 50 nm in diameter; Sigma-Aldrich) in water were obtained with a concentration of 0.01 wt.%. After thorough sonication, 2 μL/(mm^2 of sample) of dispersion was casted on VACNT/Si samples at 50ºC, leading to a uniform deposition over the whole surface, and left to dry at this temperature. (iii) The obtained NiO/VACNT samples were submitted to UV pulsed laser irradiation by means of a Brilliant B system (Quantel) in order to induce the recrystallization of NiO nanoparticles on the VACNT surface. The laser wavelength was 266 nm, the duration of the pulses was ca. 5 ns and the repetition rate was set to 10 Hz. The laser beam was expanded with a Gaussian telescope, shaped with a squared mask and then focused onto the samples by means of a convergent lens. This way, 1×1 mm^2 squared and homogeneous laser spots were obtained on the samples' surface. Areas up to 5×5 mm^2 were processed by irradiating adjacent locations with a separation distance of 1 mm. The irradiation experiments were performed in the air, at atmospheric pressure, by accumulating 100, 500, 1000 and 2000 laser pulses at different locations, each of them with 40, 80, 160 and 260 mJ cm^{-2} laser fluences.

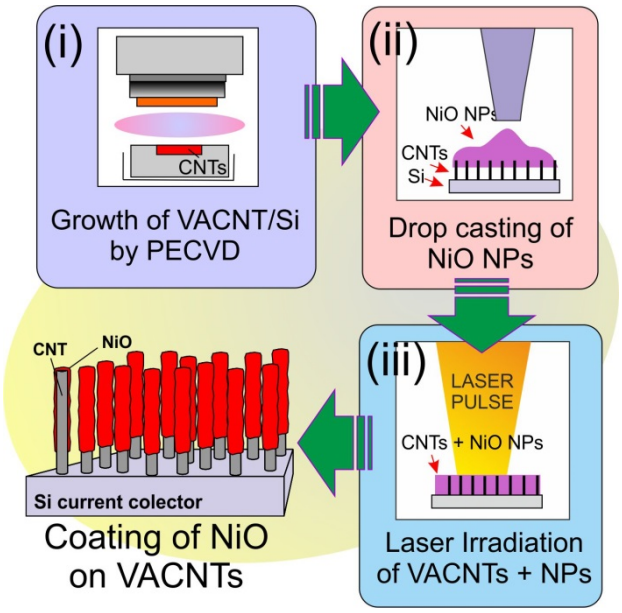

Fig. 1. Scheme of the fabrication process of NiO/VACNT samples.

Substrate			Annealing				RF-PECVD (50 W, 13.56 MHz)							
Type	RF magnetron		H_2 parameters		General parameters		Gas replacement H_2 to NH_3				C_2H_2 parameters			
	Fe (nm)	Self Bias (V)	Flow (sccm)	Pressure (Pa)	Temperature (^{0}C)	Rampe, Heating (s)	Flow (sccm)	Pressure (Pa)	Time (s)	Self Bias (V)	Flow (sccm)	Pressure (Pa)	G(t)	R
c-Si	3	-96	100	200	680	750, 120	100	80	30	-398	50	100	900	NG

Table 1. VACNT growth parameters.

The morphology of the obtained materials was characterized by field emission scanning electron microscopy (SEM) using a QUANTA 200 FEG-ESEM equipment from FEI, and extreme high resolution SEM (XHR SEM) by means of a Magellan 400L system (FEI). The structure was analyzed by high resolution transmission electron microscopy (HRTEM) and high angle annular dark field scanning TEM (HAADF-STEM) using a Tecnai F20 microscope from FEI. This equipment also allowed us to study the local composition of the samples through energy-dispersive X-ray spectroscopy (EDX). TEM specimens were prepared by carefully rubbing TEM copper grids on the NiO/VACNT samples surface. This way, the material detaches from the substrate and is deposited on the grid. Moreover, Raman spectroscopy study was carried out by a LabRAM 800 system from Horiba Jobin Yvon. Several spectra, in the 150 – 3120 cm^{-1} range, were acquired in all the samples by focusing a 532 nm laser wavelength, with a power of 1.5

mW, in spots about 500 nm in diameter. The acquisition time was set to 20 s and 3 scans per spectrum were averaged for minimizing signal noise.

3. Results and discussion

PECVD treatment leads to the growth of VACNTs, about 2-3 μm in length and up to 100 nm in diameter, totally covering the silicon surface (Fig. 2a). Most of the VACNTs exhibit a straight shape, though a fraction of them are slightly bent. The lateral distance between adjacent nanotubes varies in the range of few hundreds of nanometers. One of the most accepted models to describe the mechanism of growth of CNTs is the vapor-liquid-solid (VLS) model, proposed in 1970's by Baker et al. [38]. Although this model describes a growth mechanism for carbon filaments, it is also applicable to CNTs when metal catalyst particles are employed. Originally, the model suggests that the role of the metal particles is to form a droplet of liquid alloy, which absorbs carbon atoms until the supersaturated state is established. In our case and after reaching this state, carbon is segregated forming ordered structures molded by the Fe particle shape. In our experiments, the tubular structure of the CNTs was verified by HRTEM (Fig. 3). The type of CNT structure shown in Fig. 3b is defined as "bamboo like" because of the hollow cylindrical shape inside the nanotube. Usually, bamboo shaped nanotube consists of regular cone shaped compartments. Compartment formation in the bamboo like structure occurs because of periodic precipitation of graphite sheets on the top of catalyst particle. NH_3 can easily be dissociated due to weaker bonds compared to that of H_2. Martin S. Bell et al.[39] found bamboo-structures in nitrogen containing plasma and hollow tubes in nitrogen-free plasma. This suggests that nitrogen played critical role in compartment formation. Further, it is believed that CNT growth occurs via surface diffusion (SD) and/or bulk diffusion (BD) of carbon species through catalyst particles. High concentration of CN promoted BD of carbon through Fe particles and suppressed SD by keeping the catalyst surface clean and hence, leading to shorter compartment length. Concerning the electrochemical behavior of these structures, it has been reported that bamboo like CNTs with a higher ratio of edge-to-plane sites along its surface, show a higher electronic transfer than the straight, hollow CNTs for electrochemical experiments [40,41]. There is a possibility of CN diffusion through the Fe particles as well [39]. But CN or N have very limited solubility in Fe so the concentration of N or

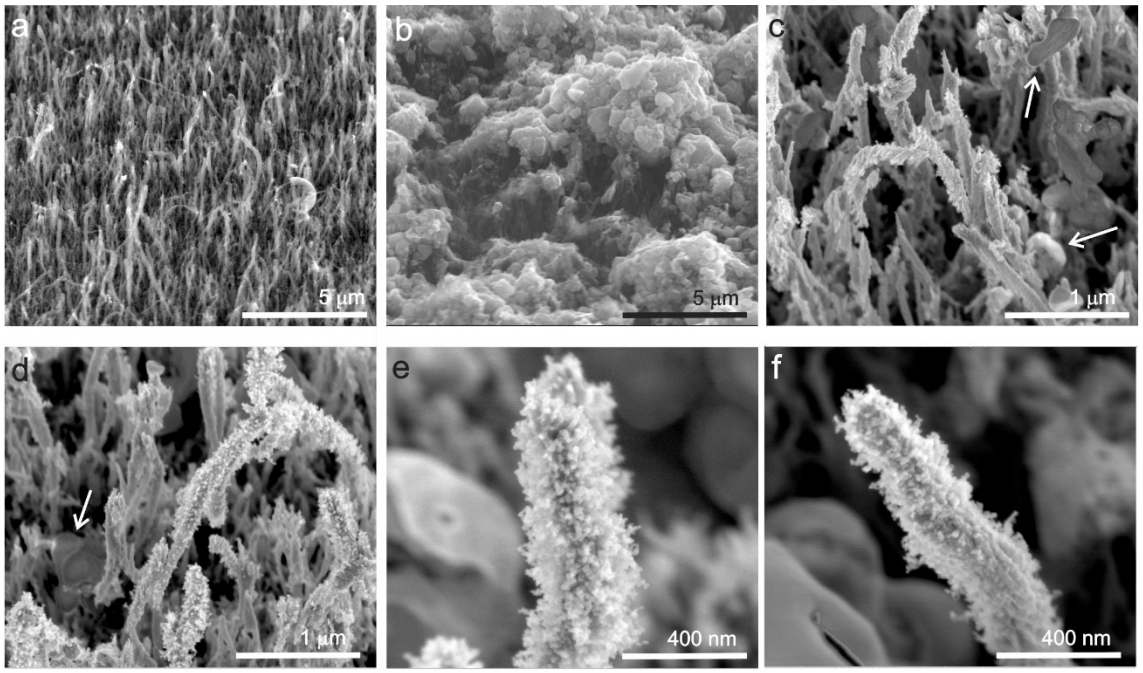

Fig. 2. Scanning electron microscope images of (a) as grown VACNTs, (b) NiO nanoparticles deposited on VACNTs, and details of the samples obtained at (c) 80 mJ cm^{-2} after accumulation of 500 pulses, and 160 mJ cm^{-2} accumulating (d, e) 500 and (f) 1000 laser pulses. Arrows in (c) and (d) point to the excess NiO clusters.

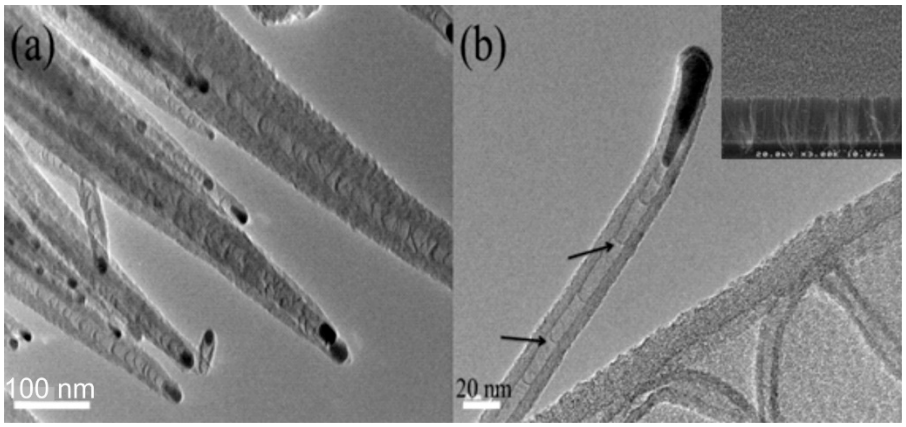

Fig. 3. HRTEM images of PECVD grown multiwalled CNTs. (a) CNTs with catalyst on their top surfaces. The side walls of CNTs contain amorphous carbon, which is a by-product deposited during the PECVD growth. (b) Elongated catalyst particle (Fe) at the tip of the CNT, which clearly evidences the CNT growth mechanism. The arrows inside the nanotube point to the graphene transversal layers inside the nanotube at regular

distances. The micrograph on the upper right corner shows the image of the CNTs mat grown by PECVD on p-Si wafers.

CN in Fe is supposed to be very low compared to carbon. Outer diameter of growing tube is confined by the size of the catalyst particle. The shape of the tip is controlled by the local geometry of the catalyst particle seeding the growth of the tube [42]. The production of nanotubes requires a controlled deposition of carbon, which can then self-assemble into an energetically favored nanotube form. This controlled deposition rate is achieved through the combination of two reactions: the dissociation of a carbon-rich gas (in our case, C_2H_2) and the removal of excess carbon, which would otherwise lead to amorphous carbon deposits. The main role of NH_3 in the growth phase of CNT was to prevent the formation of amorphous carbon and dilute the C_2H_2. At high NH_3 ratios, NH_3 decomposes preferentially over C_2H_2 due to the relative weakness of its molecular bonds. This allows the C_2H_2 to decompose slowly, generating the controlled amounts of carbon necessary for nanotube formation and giving rise to clean, well-aligned carbon nanotubes. At high C_2H_2 ratios, there is insufficient NH_3 to effectively suppress C_2H_2 decomposition, resulting in higher levels of carbon generation and the deposition of amorphous carbon onto the substrate. NH_3 has a key role in removing any excess of carbon through the generation of reactive atomic hydrogen [43]. XPS analysis of the VACNTs presents a nitrogen concentration of about 4.3% due to the use of ammonia during growth [37]. The main form of this nitrogen is pyridinic and aliphatic amine.

Fig. 2b shows the VACNT surface after the drop casting deposition and drying of the NiO NPs. As observed, NiO NPs appear highly aggregated leading to the formation of a non-uniform layer, with hundreds of nanometers to micron range thickness, covering the VACNT surface. It should be remarked that, due to the large aggregation of the NPs into hundreds of nanometers clusters, most of the voids between the CNTs seem to not be completely filled of NPs. The optical absorption coefficient of NiO at 266 nm wavelength (4.7 eV photon energy) is ca. 5×10^5 cm^{-1} [44], being the corresponding optical penetration depth about 200 nm. Thus, the laser radiation is mainly absorbed in NiO film with thickness larger than this value. The radiation is also absorbed by the CNTs in the zones with low coverage of NiO. It has to be noticed that the reported Ni-O bond dissociation energy is about 392 kJ mol^{-1} (ca. 4.1 eV/bond) [45] which is

comparable to the UV photon energy. Consequently, laser irradiation of NiO NPs might cause their direct chemical decomposition and light-induced reactivity with surrounding chemical species (photochemical mechanisms). Subsequently, the deposited energy would transform to thermal one leading to the fast increase of the temperature in the material with each laser pulse. SEM studies reveal that laser irradiation of NiO/VACNT system at low 40 mJ cm^{-2} fluence does not lead to remarkable modification of the morphology in the whole range of accumulated pulses. However, irradiation at higher laser fluences provokes significant change of the treated material, being more pronounced as the accumulation of laser pulses proceeds. The material irradiated with 80 mJ cm^{-2} laser fluence shows VACNTs coated with irregular layer at the surface of their outer walls up to 2 μm in depth. Between them hundreds of nm sized spherical particles can be identified (Fig. 2c; Fig. S1, Supporting Information). The characteristic shape of these particles points to melting-merging and resolidification processes of excess NiO NPs into larger clusters (arrows in Fig. 2c, d). Due to the absence of the initial NiO layer on the top of the VACNT forest, it can be assumed that, during laser-driven heating, the top NiO layer is molten and flows on the CNT outer surface, covering them. Thus, the irregular surface morphology observed on CNTs would be due to the deposition of a NiO continuous coating on them. Interestingly, the accumulation of 2000 pulses with 80 mJ cm^{-2} laser fluence, or even at just 100 pulses with 160 mJ cm^{-2} fluence leads to the formation of an extended structure in the radial direction of the NiO/VACNTs giving them a “spiky” aspect (Figs. 2d, e). The accumulation of laser pulses provokes the proliferation of “spiky” CNTs and the quantity of these features on the carbon nanotubes. However, a shortening of these structures and the formation of a kind of granular coating on the CNTs is observed beyond 1000 pulses with 160 mJ cm^{-2} fluence (Fig. 2f; Fig. S2, Supporting Information). Further accumulation of pulses at this laser fluence, or higher, up to 260 mJ cm^{-2} provokes the partial melting and collapse of the CNTs.

Due to the greater effective area of “spiky” NiO/VACNT structures and their potential interest for electrochemical applications, further investigation of their structure is carried out. Fig. 4 shows HAADF-STEM images (Z-contrast) of NiO/VACNT processed applying 500 laser pulses at 160 mJ cm^{-2} fluence. As observed, VACNTs are totally decorated with NPs, about few to 30 nm in size. EDX spectra reveal the presence of Ni, O, C, Cu and less intense Fe signal in the NPs (Fig. 4c). The Fe signal arises from

the residue of catalyzer used in the PECVD growth of the VACNTs, and the C and Cu signals come from the nanotube and TEM grid, respectively. Thus, it could be pointed out that the observed NPs are mainly composed of NiO. It must be reminded that the initial diameter of the NiO NPs is around 50 nm. The presence of much smaller NiO

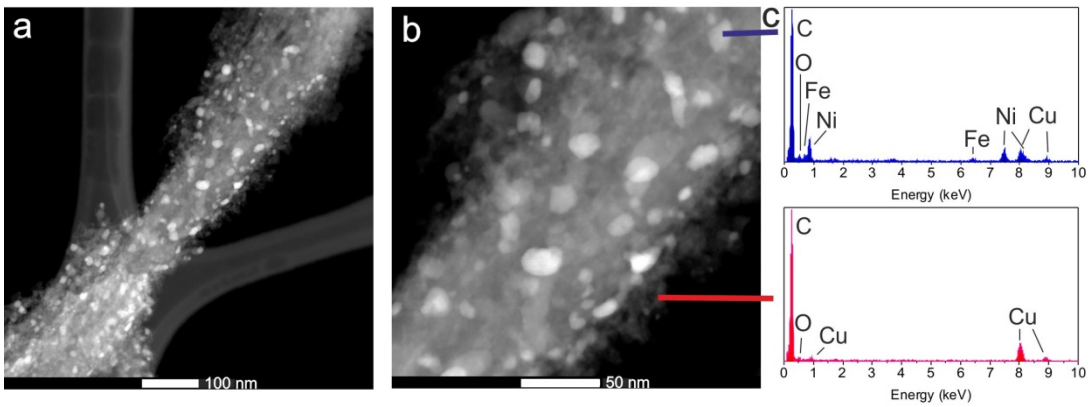

Fig. 4. (a, b) High angle annular dark field (Z-contrast) STEM images of NiO/VACNT obtained by accumulation of 500 laser pulses at 160 mJ cm^{-2}. (c) Typical EDX signals in (up) a nanostructure and (down) in the VACNT wall.

NPs on the CNT surface would support the proposed laser-induced melting, flowing and recrystallization mechanisms. Besides, protrusions located on the VACNT surface, which show less contrast than NPs, do not show any sign of metals and only contain C and a tiny quantity of O. These zones would be ascribed to carbon nanotubes' structure. HRTEM analyses are carried out in the same sample for the study of the crystalline structure of the material submitted to irradiation. Fig. 5a shows the TEM image of the same location presented in Fig. 4b for comparison. High resolution images reveal that the NPs are crystalline, since parallel planes domains are observed inside them. The interplanar spacing can be calculated at these domains by fast Fourier transform (FFT). Thus, at locations indicated by arrows in Fig. 5b, interplanar distances of 0.21 and 0.24 nm are measured, corresponding respectively to (200) and (111) planes of cubic NiO (Bunsenite; JCPDS 00-047-1049) [46]. At other locations, at about 5 nm distance inside the NPs additional planes with 0.14, 0.19 and 0.41 nm spacing, corresponding to (220), (210) and (100) planes of NiO are recorded (not shown). The combination of planes and their orientation change inside the NPs is a clear indication of their polycrystalline nature. In addition to the NiO nanostructures, the outer graphitic planes of the CNTs

appear distorted and intertwined in many sites (arrows in Fig. 5c), indicating the development of high thermal stress and the creation of defects in the VACNT structure. No significant flaws are observed in the inner part of the CNTs. Previous works report the formation of different types of damage in CNT submitted to laser irradiation [47,48]. Furthermore, profuse laser-induced effects can lead to complex structural modifications such as unzipping of CNT to graphene nanoribbons, and even their transformation to polymers [49,50].

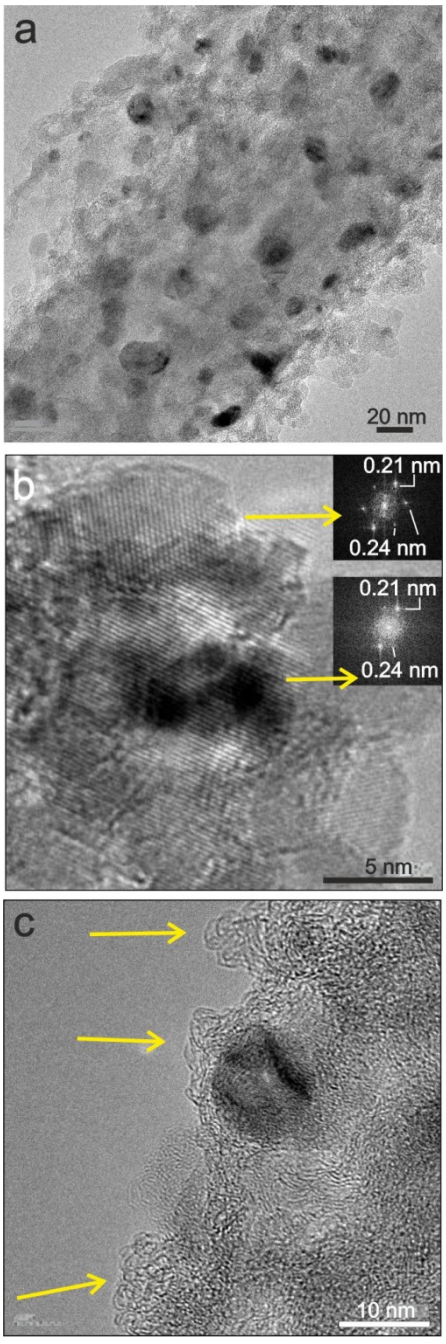

Fig. 5. HRTEM images of NiO/VACNTs irradiated with 160 mJ cm^{-2} fluence and accumulating 500 pulses. (b) Includes FFT patterns of the marked zones. The arrows in (c) point to twisted graphene sheets.

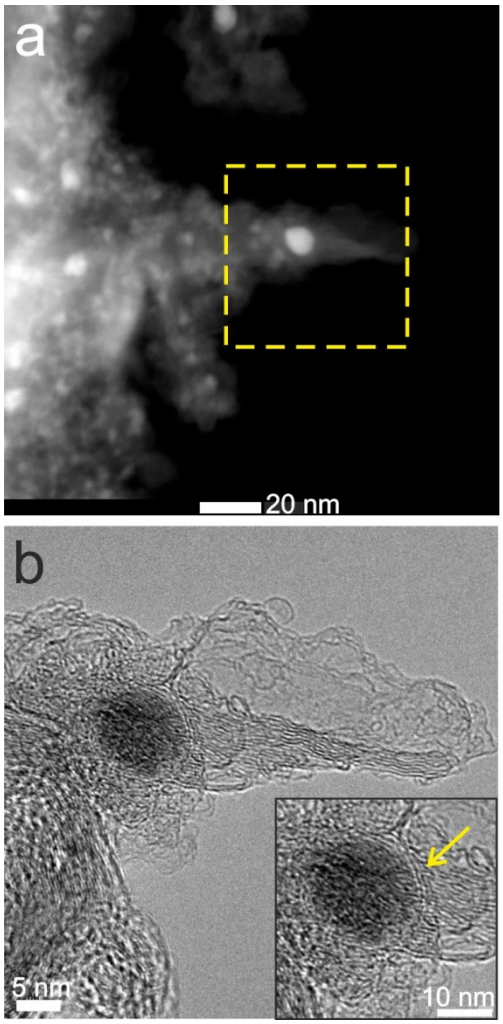

Fig. 6. (a) STEM and (b) HRTEM images of a protrusion located in a NiO/VACNT irradiated with 160 mJ cm^{-2} fluence and accumulating 500 pulses. The arrow in (b) indicates graphitic planes surrounding a NiO nanostructure.

The spiky structures that appear at the VACNT surface are also specifically studied by TEM (Fig. 6). As observed, these nanostructures can extend several tens of nanometers in length and are constituted by both NiO and carbon features. Interestingly, high resolution TEM reveals that they are composed of beams of graphitic planes which appear to grow from NiO NPs. Additionally, parallel graphene planes are also observed

nearby the NiO nanostructures, surrounding their surface to some extent (see arrow in Fig. 6b). These facts would point to the reconstruction of the CNT graphitic shells influenced by the action of the high temperatures and the catalytic activity of NiO nanostructures. Probably, carbon nanotube would remain in solid state in this process, since melting would lead to its amorphization [34]. Although the catalytic behavior of nickel during the growth of carbon nanotubes is well known [1], the catalytic effect of NiO is less studied, and only some works about the NiO-assisted growth of carbon nanostructures are reported [51-53]. It is worth noticing that the catalytic growth of sp^2-hybridized carbon materials is normally accomplished in vapor phase. In this case, reactant molecules (generally hydrocarbons) have significant mobility and decompose when interacting with the hot catalyst, leading to the surface / bulk diffusion of carbon atoms and further growth of graphitic shells. Interestingly, this work suggests that NiO nanostructures inserted in VACNTs could drive the solid state reconstruction of graphitic shells by means of photochemical-photothermal mechanisms when irradiated with ultraviolet laser pulses. In particular, the photochemically-induced brief decomposition of NiO to Ni species could lead to high reactivity and enhanced catalytic action with each laser pulse.

In order to get more understanding on the physical mechanisms taking place, thermal simulations of idealized NiO/VACNT structures irradiated with a UV laser pulse is carried out (Fig. 7). The structures used in the model are composed of VACNTs 2 μm long and 100 nm in diameter on silicon substrate: one VACNT stands alone (CNT), another one has a 20 nm-sized NiO nanostructure (NS) on the top-side (CNT-NiO NS), and the last one is coated with a 20 nm-thick NiO layer (CNT-NiO layer) (Fig. 7a). The designated size for simulated NiO NS and layer (20 nm) is a representative size of NiO nanostructures' observed on VACNT surface (Fig. 5a). The numerical calculations are carried out by means of the finite element method, solving the 2D heat equation in the described assemblies using COMSOL 5.2 software. For the sake of simplicity, the model neglects the effects of nanometric dimensions in heat transport and optical properties, and only considers photothermal processes. The optical and thermal properties of VACNTs, NiO and Si materials are taken from Refs. [34,44,54]. The pulsed laser radiation, considered to be incident from the top part of the structures, is absorbed at the top CNTs and NiO surfaces leading to the heating of the whole assemblies in the nanosecond regime, given the small size and high thermal

conductivity of the involved materials. As observed in Fig. 7b, the laser pulse provokes the development of rapid thermal cycles in the modelled features. The achieved maximum temperatures become higher with the laser fluence: whereas temperature rises to ca. 700 K at 80 mJ cm^{-2}, up to about 1200 K is obtained at 160 mJ cm^{-2}. As expected,

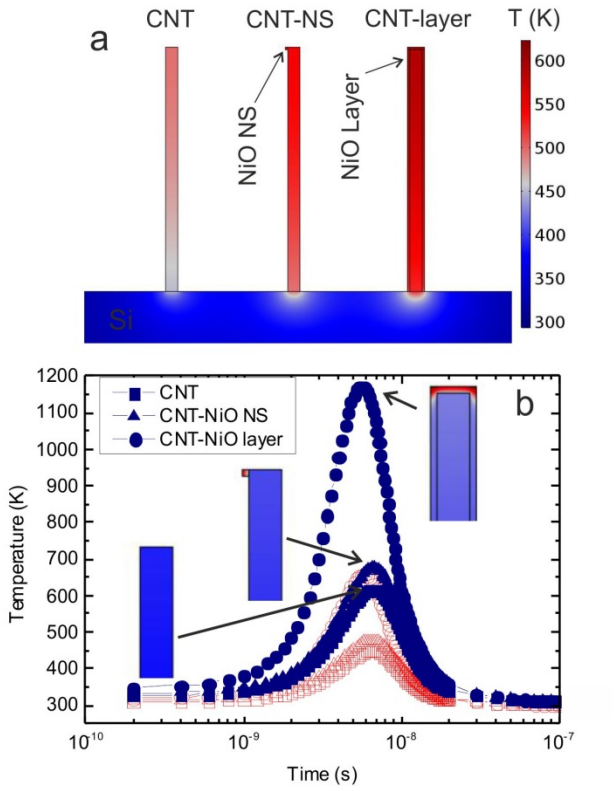

Fig. 7. (a) Simulated temperature distribution in CNT, CNT-NiO NS and CNT-NiO layer assemblies irradiated with 160 mJ cm^{-2} laser pulse at 10 ns. (b) Temperature evolution with time on a surface point of CNT, CNT-NiO NS and CNT-NiO layer assemblies irradiated with 80 mJ cm^{-2} (open symbols) and 160 mJ cm^{-2} (solid symbols) pulses. Insets: Details of temperature distributions at structures irradiated with 160 mJ cm^{-2} at 6 ns.

the maximum temperatures remain far below the CNT and NiO melting temperatures, considered to be ca. 4800 K and 2230 K, respectively. Nonetheless, the developed temperature range can change significantly depending on the relative angle between CNTs and laser beam incidence axis [34]. Since the absorption coefficient of NiO is more than ten-fold higher than the one of carbon nanotube, the modelled NiO/VACNT assemblies reach slightly higher temperatures than the VACNT one. As it can be

observed in CNT-NiO NS, the NiO nanostructure acts as an absorbing center reaching quite large temperatures (inset in Fig. 7b). Nevertheless, the overall temperature of the CNT-NiO NS is just a few tens of degrees higher than the VACNT alone. This phenomenon is more noticeable in the CNT-NiO layer assembly which points to the development of higher temperatures with greater NiO coverage of the carbon nanotubes. Evidently, the maximum temperature also increases with the thickness of the NiO layer / nanostructure. Therefore, under the action of cumulative laser pulses, initial thick enough NiO nanostructures (or continuous layer) covering the VACNTs reach melting temperature and undergo flowing and dewetting along the CNT surface, leading to the formation of smaller NiO features (initial process of melting and dewetting achieved with the first laser pulses is not simulated). Since melting temperature of graphitic carbon is much higher than that of NiO, no melting of CNTs is expected, though high temperatures, probably assisted by photochemical mechanisms, would trigger the creation and migration of structural defects at CNT graphitic shells [34,55]. Further irradiation leads to the heating without melting of the small NiO particles besides the surrounding carbon material to several hundreds of degrees, provoking the thermally-activated diffusion of nearby carbon atoms and the catalytic recrystallization of graphitic shells around NiO, leading to the growth of the spiky features.

Raman spectroscopy measurements of NiO/VACNT samples are expected to provide additional insight into the structural properties of the constituent materials. Fig. 8a depicts characteristic spectra of non-irradiated NiO/VACNT film after NiO NPs deposition and drying, as well as one film irradiated by accumulation of 500 pulses with 160 mJ cm^{-2} laser fluence. The presence of intense bands centered at around 490, 1100, 1360 and 1590 cm^{-1} is revealed. After deconvolution process, the broad band centered at 1100 cm^{-1} can be considered to be composed of two bands, centered at about 980 and 1120 cm^{-1}. Moreover, an additional band appears at ca. 1500 cm^{-1}. The bands located at 490, 980, 1120 and 1500 cm^{-1} can be ascribed to one-phonon (1P), two-phonon (2P) and two-magnon (2M) scattering at NiO nanostructures (Fig. 8a) [56]. The bands located at 1360 and 1590 cm^{-1} are respectively attributed to the disorder-induced (D) and graphitic (G) bands of VACNTs [57]. As observed, 1P NiO band is the dominating one in the spectrum of non-irradiated NiO/VACNT sample. However, after irradiation, the intensity of NiO bands, especially 1P, significantly decreases whereas the relative intensity of VACNT bands increases as compared to NiO ones. This effect is easily

discernible in Fig. 8b, where the NiO (1P)-to-G band intensity ratio is calculated. As observed, NiO (1P) / G ratio in non-irradiated NiO/VACNT sample exhibits large range of values due to the variable thickness of the deposited NiO NPs film. However, when irradiated, the range of NiO/G calculated values is confined to smaller values. The NiO

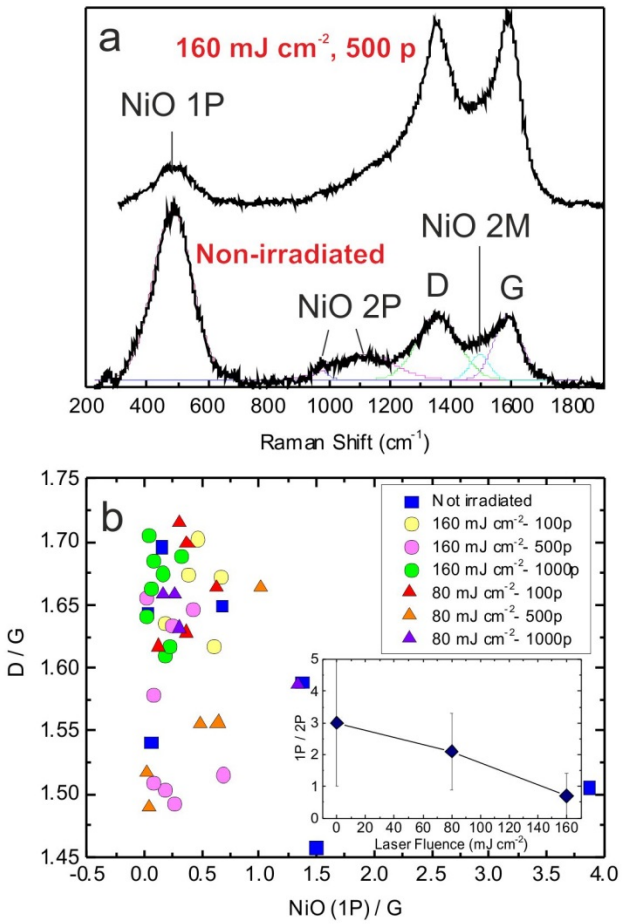

Fig. 8. (a) Typical Raman spectra obtained in non-irradiated NiO/VACNT sample and after accumulation of 500 laser pulses at 160 mJ cm^{-2}. (b) Plot of the D/G versus NiO (1P)/G intensity relations in samples irradiated with 80 and 160 mJ cm^{-2}. Inset: Evolution of the 1P/2P (1120 cm^{-1}) area relation versus laser fluence after the submission of 1000 laser pulses.

bands intensity decrease is mainly due to the decrease of the NiO layer thickness after laser irradiation, as confirmed by SEM analyses (Fig. 2). Besides, it has been previously reported that no first-order Raman scattering is expected in the paramagnetic phase of

NiO with the NaCl structure. Nevertheless, when NiO contains high density of structural flaws or becomes antiferromagnetically ordered, the intensity of 1P band considerably increases [58]. Thus, the relation of 1P (490 cm^{-1}) over 2P (1120 cm^{-1}) bands areas could account to the nickel oxide crystallinity, decreasing with the increase of the crystalline quality. Inset in Fig. 8b shows the evolution of the mean value of 1P/2P ratio of non-irradiated sample as well as the ones submitted to 1000 laser pulses at 80 and 160 mJ cm^{-2}. As observed, 1P/2P ratio decreases with the increase of the laser fluence from about 3 in non-irradiated sample to around 2 when irradiated with 80 mJ cm^{-2}, where an irregular and continuous NiO film is observed on the top of the VACNTs (Fig. 2c). At the sample processed with 160 mJ cm^{-2}, composed of "spiky" NiO/VACNTs, containing polycrystalline NiO crystals (Fig. 5b), 1P/2P ratio clearly decreases to ca. 0.7, indicating better crystallinity as compared to the initial NiO NPs.

Furthermore, we studied the evolution of the D and G Raman bands of VACNTs. D band is related to structural defects/disorder and G mode arises from sp^2-bonded carbon atoms. Thus, the D/G intensity ratio is generally used as a figure of merit of the flaw content in the CNTs structure [59]. As revealed in Fig. 8b, non-irradiated NiO/VACNT shows D/G values in range of 1.45-1.70. The relatively wide range of D/G values indicates the growth of VACNTs with varied degree of structural defects. This fact is commonly present in CVD-grown CNTs since their nucleation highly depends on elements as the catalyst crystallographic properties provoking great impact in the growth and defect concentration levels in the resulting CNT material [60-62]. Samples submitted to laser irradiation at 80 and 160 mJ cm^{-2} reveal D/G ratios amidst the initial ones. Indeed, D/G values seem to be independent of laser irradiation conditions and relative amount of NiO-to-CNTs (NiO/G), to some extent. Previous works show that rapid high-temperature annealing treatments can induce the graphitization of CNTs, leading to D/G decrease, even though above a temperature threshold the creation of structural defects is provoked, accounting for a D/G augment [63]. Furthermore, UV laser irradiation of MWCNTs performed in N_2 atmosphere in conditions in which substantial melting and amorphization of CNT structure is accomplished leads to notable D/G reduction [34]. Therefore, similar D/G ratios of laser irradiated NiO/VACNT samples as compared to non-irradiated ones reveal that the laser-induced modifications and defects of VACNTs observed in the CNT structure by TEM (Figs. 5, 6) are not widely extended. Moreover, electron microscopy inspections revealed that the

main structural integrity of the VACNTs is preserved and the defects seem to be mainly located in the surface, where carbon material highly interacts with NiO and oxygen from the surrounding atmosphere.

4. Conclusion

UV pulsed laser irradiation of VACNT forests coated with NiO NPs has been carried out in ambient conditions. The accumulation of laser pulses induces the cyclic rapid heating of the NiO and CNT materials, provoking the melting of NiO NPs beyond a laser fluence threshold. Molten NiO flows on the CNT surface and, after cooling-crystallization, creates different NiO/VACNT configurations depending on the experimental conditions. At low fluence, a continuous NiO layer is formed, leading to an extended coating of VACNTs. More energetic processing leads to breaking-up of the NiO liquid layer and the formation of nanometric-sized NiO nanostructures covering the VACNT surface. Besides, prickly structures appear covering the CNT surfaces. These nanostructures, up to few tens of nanometers long, are composed of parallel beams of graphitic shells that seem to propagate from NiO structures. The origin of these features could be the reconstruction of carbon material by the action of the developed high temperatures and NiO catalytic interactions, probably assisted by photochemical processes. Pulsed laser irradiation of NiO-CNT systems has been demonstrated to be capable to create remarkable nanostructures by the activation of complex and coupled phenomena. The development of such kind of NiO/VACNT structures, which could significantly increase the active area and electrochemical properties of the processed materials, could lead to the development of enhanced functional devices in a relatively easy, cheap and non-toxic way.

Acknowledgement

The authors acknowledge the financial support of the Spanish Ministry of Economy and Competitiveness under the projects MAT2010-20468, ENE2014-56109-C3-1-R and ENE2014-56109-C3-3-R, as well as AGAUR (Generalitat de Catalunya) under the project 2014SGR984. ICMAB acknowledges financial support from the Spanish Ministry of Economy and Competitiveness, through the “Severo Ochoa” Programme for

Centres of Excellence in R&D (SEV- 2015-0496). The authors would also like to thank the CCiT-UB for help with the structural and morphological characterization.

References

1. Cherusseri J, Kar KK (2015) Self-standing carbon nanotube forest electrodes for flexible supercapacitors. Rsc Advances 5 (43):34335-34341. doi:10.1039/c5ra04064g
2. Hsia B, Marschewski J, Wang S, In JB, Carraro C, Poulikakos D, Grigoropoulos CP, Maboudian R (2014) Highly flexible, all solid-state micro-supercapacitors from vertically aligned carbon nanotubes. Nanotechnology 25 (5). doi:10.1088/0957-4484/25/5/055401
3. Jung HY, Hong S, Yu A, Jung SM, Jeoung SK, Jung YJ (2015) Efficient lithium storage from modified vertically aligned carbon nanotubes with open-ends. Rsc Advances 5 (84):68875-68880. doi:10.1039/c5ra14263f
4. Liatard S, Benhamouda K, Fournier A, Ramos R, Barchasz C, Dijon J (2015) Vertically-aligned carbon nanotubes on aluminum as a light-weight positive electrode for lithium-polysulfide batteries. Chemical Communications 51 (36):7749-7752. doi:10.1039/c4cc08848d
5. De Luca A, Cole MT, Hopper RH, Boual S, Warner JH, Robertson AR, Ali SZ, Udrea F, Gardner JW, Milne WI (2015) Enhanced spectroscopic gas sensors using in-situ grown carbon nanotubes. Applied Physics Letters 106 (19). doi:10.1063/1.4921170
6. Saheed MSM, Mohamed NM, Burhanudin ZA (2014) Optimum design of ionization-based gas sensor using vertically aligned multiwalled carbon nanotubes array. Sensors and Actuators B-Chemical 199:232-238
7. Nick C, Yadav S, Joshi R, Schneider JJ, Thielemann C (2015) A three-dimensional microelectrode array composed of vertically aligned ultra-dense carbon nanotube networks. Applied Physics Letters 107 (1)
8. Penza M, Rossi R, Alvisi M, Signore MA, Cassano G, Dimaio D, Pentassuglia R, Piscopiello E, Serra E, Falconieri M (2009) Characterization of metal-modified and vertically-aligned carbon nanotube films for functionally enhanced gas sensor applications. Thin Solid Films 517 (22):6211-6216
9. Yang Z, Zhou XM, Nie HG, Yao Z, Huang SM (2011) Facile Construction of Manganese Oxide Doped Carbon Nanotube Catalysts with High Activity for Oxygen Reduction Reaction and Investigations into the Origin of their Activity Enhancement. Acs Applied Materials & Interfaces 3 (7):2601-2606
10. Reddy ALM, Shaijumon MM, Gowda SR, Ajayan PM (2009) Coaxial MnO2/Carbon Nanotube Array Electrodes for High-Performance Lithium Batteries. Nano Letters 9 (3):1002-1006
11. Liu JW, Essner J, Li J (2010) Hybrid Supercapacitor Based on Coaxially Coated Manganese Oxide on Vertically Aligned Carbon Nanofiber Arrays. Chemistry of Materials 22 (17):5022-5030
12. Yang Z, Zhou X, Jin Z, Liu Z, Nie H, Chen Xa, Huang S (2014) A Facile and General Approach for the Direct Fabrication of 3D, Vertically Aligned Carbon Nanotube Array/Transition Metal Oxide Composites as Non-Pt Catalysts for Oxygen Reduction Reactions. Advanced Materials 26 (19):3156-3161. doi:10.1002/adma.201305513
13. Amade R, Vila-Costa M, Hussain S, Casamayor EO, Bertran E (2015) Vertically aligned carbon nanotubes coated with manganese dioxide as cathode material for microbial fuel cells. Journal of Materials Science 50 (3):1214-1220. doi:10.1007/s10853-014-8677-2
14. Kalubarme RS, Kim YH, Park CJ (2013) One step hydrothermal synthesis of a carbon nanotube/cerium oxide nanocomposite and its electrochemical properties. Nanotechnology 24 (36)

15. Abbas SM, Ali S, Niaz NA, Ali N, Ahmed R, Ahmad N (2014) Superior electrochemical performance of mesoporous Fe3O4/CNT nanocomposites as anode material for lithium ion batteries. Journal of Alloys and Compounds 611:260-266. doi:10.1016/j.jallcom.2014.05.103
16. Jung D, Han M, Lee GS (2014) Gas-sensing properties of multi-walled carbon-nanotube sheet coated with NiO. Carbon 78:156-163. doi:10.1016/j.carbon.2014.06.063
17. Chen N, Li Q, Li Y, Deng D, Xiao X, Wang Y (2015) Facile synthesis and gas sensing performances based on nickel oxide nanoparticles/multi-wall carbon nanotube composite. Journal of Materials Science-Materials in Electronics 26 (10):8240-8248. doi:10.1007/s10854-015-3487-0
18. Prasad R, Bhat BR (2015) Multi-wall carbon nanotube-NiO nanoparticle composite as enzyme-free electrochemical glucose sensor. Sensors and Actuators B-Chemical 220:81-90
19. Cheng J, Zhao B, Zhang W, Shi F, Zheng G, Zhang D, Yang J (2015) High-Performance Supercapacitor Applications of NiO-Nanoparticle-Decorated Millimeter-Long Vertically Aligned Carbon Nanotube Arrays via an Effective Supercritical CO2-Assisted Method. Advanced Functional Materials 25 (47):7381-7391. doi:10.1002/adfm.201502711
20. Wu M-S, Zheng Y-R, Lin G-W (2014) Three-dimensional carbon nanotube networks with a supported nickel oxide nanonet for high-performance supercapacitors. Chemical Communications 50 (60):8246-8248. doi:10.1039/c4cc02725f
21. Zhang J, Yi X-b, Wang X-C, Ma J, Liu S, Wang X-J (2015) Nickel oxide grown on carbon nanotubes/carbon fiber paper by electrodeposition as flexible electrode for high-performance supercapacitors. Journal of Materials Science-Materials in Electronics 26 (10):7901-7908. doi:10.1007/s10854-015-3442-0
22. Susantyoko RA, Wang X, Xiao Q, Fitzgerald E, Zhang Q (2014) Sputtered nickel oxide on vertically-aligned multiwall carbon nanotube arrays for lithium-ion batteries. Carbon 68:619-627. doi:10.1016/j.carbon.2013.11.041
23. Lalia BS, Khalil A, Shah T, Hashaikeh R (2015) Flexible carbon nanostructures with electrospun nickel oxide as a lithium-ion battery anode. Ionics 21 (10):2755-2762. doi:10.1007/s11581-015-1482-3
24. Ma YF, Sheng LM, Zhao HB, An K, Yu LM, Xu JQ, Zhao XL (2015) Synthesis of NiO/carbon shell/single-walled carbon nanotube composites as anode materials for lithium ion batteries. Solid State Sci 46:49-55
25. Yu X, Hua T, Liu X, Yan Z, Xu P, Du P (2014) Nickel-Based Thin Film on Multiwalled Carbon Nanotubes as an Efficient Bifunctional Electrocatalyst for Water Splitting. Acs Applied Materials & Interfaces 6 (17):15395-15402. doi:10.1021/am503938c
26. Huang J, Zhu N, Yang T, Zhang T, Wu P, Dang Z (2015) Nickel oxide and carbon nanotube composite (NiO/CNT) as a novel cathode non-precious metal catalyst in microbial fuel cells. Biosensors & Bioelectronics 72:332-339. doi:10.1016/j.bios.2015.05.035
27. Jiang S, Handberg ES, Liu F, Liao Y, Wang H, Li Z, Song S (2014) Effect of doping the nitrogen into carbon nanotubes on the activity of NiO catalysts for the oxidation removal of toluene. Applied Catalysis B-Environmental 160:716-721. doi:10.1016/j.apcatb.2014.06.026
28. Bashir SM, Hossain SS, Rahman SU, Ahmed S, Hossain MM (2015) NiO/MWCNT Catalysts for Electrochemical Reduction of CO2. Electrocatalysis 6 (6):544-553. doi:10.1007/s12678-015-0270-1
29. Maeng J, Heo S, Jo G, Choe M, Kim S, Hwang H, Lee T (2009) The effect of excimer laser annealing on ZnO nanowires and their field effect transistors. Nanotechnology 20 (9)
30. Perez del Pino A, Gyoergy E, Marcus IC, Roqueta J, Alonso MI (2011) Effects of pulsed laser radiation on epitaxial self-assembled Ge quantum dots grown on Si substrates. Nanotechnology 22 (29). doi:295304

10.1088/0957-4484/22/29/295304

31. Perez del Pino A, Gyoergy E, Logofatu C, Puigmarti-Luis J, Gao W (2015) Laser-induced chemical transformation of graphene oxide-iron oxide nanoparticles composites deposited on polymer substrates. Carbon 93:373-383. doi:10.1016/j.carbon.2015.05.078
32. del Pino AP, Gyorgy E, Cotet C, Baia L, Logofatu C (2016) Laser-induced chemical transformation of free-standing graphene oxide membranes in liquid and gas ammonia environments. Rsc Advances 6 (55):50034-50042
33. del Pino AP, Datcu A, Gyorgy E (2016) Direct multipulse laser processing of titanium oxide-graphene oxide nanocomposite thin films. Ceramics International 42 (6):7278-7283
34. Perez del Pino A, Gyoergy E, Cabana L, Ballesteros B, Tobias G (2014) Ultraviolet pulsed laser irradiation of multi-walled carbon nanotubes in nitrogen atmosphere. Journal of Applied Physics 115 (9). doi:10.1063/1.4864776
35. Zhang Y, Gong T, Wei J, Liu W, Wang K, Wu D (2007) Structural changes in double-walled carbon nanotube strands induced by ultraviolet laser irradiation. Journal of Physical Chemistry C 111 (7):2901-2905. doi:10.1021/jp0666838
36. Kichambare PD, Chen LC, Wang CT, Ma KJ, Wu CT, Chen KH (2001) Laser irradiation of carbon nanotubes. Materials Chemistry and Physics 72 (2):218-222. doi:10.1016/s0254-0584(01)00440-0
37. Hussain S, Amade R, Jover E, Bertran E (2013) Nitrogen plasma functionalization of carbon nanotubes for supercapacitor applications. Journal of Materials Science 48 (21):7620-7628
38. Baker RTK, Yates DJC, Dumesic JA (1982) Filamentous Carbon Formation over Iron Surfaces. Acs Sym Ser 202:1-21
39. Bell MS, Teo KBK, Lacerda RG, Milne WI, Hash DB, Meyyappan M (2006) Carbon nanotubes by plasma-enhanced chemical vapor deposition. Pure Appl Chem 78 (6):1117-1125
40. Zhu JT, Jia JC, Kwong FL, Ng DHL (2012) Synthesis of bamboo-like carbon nanotubes on a copper foil by catalytic chemical vapor deposition from ethanol. Carbon 50 (7):2504-2512
41. del Campo FJ, Garcia-Cespedes J, Munoz FX, Bertran E (2008) Vertically aligned carbon nanotube based electrodes: Fabrication, characterisation and prospects. Electrochem Commun 10 (9):1242-1245
42. Srivastava SK, Vankar VD, Kumar V (2006) Growth and microstructures of carbon nanotube films prepared by microwave plasma enhanced chemical vapor deposition process. Thin Solid Films 515 (4):1552-1560
43. Bell MS, Teo KBK, Milne WI (2007) Factors determining properties of multi-walled carbon nanotubes/fibres deposited by PECVD. Journal of Physics D-Applied Physics 40 (8):2285-2292
44. Newman R, Chrenko RM (1959) Optical Properties of Nickel Oxide. Phys Rev 114 (6):1507-1513
45. Dean JA (1999) Lange's Handbook of Chemistry. McGraw-Hill, New York
46. Makhlouf SA (2008) Electrical properties of NiO films obtained by high-temperature oxidation of nickel. Thin Solid Films 516 (10):3112-3116
47. Jeschke HO, Diakhate MS, Garcia ME (2009) Molecular dynamics simulations of laser-induced damage of nanostructures and solids. Applied Physics a-Materials Science & Processing 96 (1):33-42
48. Mases M, Noel M, Dossot M, McRae E, Soldatov AV (2011) Laser-induced damage and destruction of HiPCO nanotubes in different gas environments. Phys Status Solidi B 248 (11):2540-2543
49. Kumar P, Panchakarla LS, Rao CNR (2011) Laser-induced unzipping of carbon nanotubes to yield graphene nanoribbons. Nanoscale 3 (5):2127-2129
50. Hakamatsuka M, Yoshimura H, Tachibana M (2011) Formation of trans-polyacetylene from single-wall carbon nanotubes. Carbon 49 (6):1869-1872
51. Lin HN, Chang YH, Yen JH, Hsu JH, Leu IC, Hon MH (2004) Selective growth of vertically aligned carbon nanotubes on nickel oxide nanostructures created by atomic force microscope nano-oxidation. Chemical Physics Letters 399 (4-6):422-425

52. Hsu HL, Jehng JM, Liu YC (2009) Synthesis and characterization of carbon nanotubes synthesized over NiO/Na-montmorillonite catalyst and application to a hydrogen peroxide sensor. Materials Chemistry and Physics 113 (1):166-171
53. Gong J, Liu J, Chen XC, Jiang ZW, Wen X, Mijowska E, Tang T (2014) Striking influence of NiO catalyst diameter on the carbonization of polypropylene into carbon nanomaterials and their high performance in the adsorption of oils. Rsc Advances 4 (64):33806-33814
54. J. E. Keem JMH (1978) Selected electrical and thermal properties of undoped nickel oxide. vol 52. Alexandria
55. Gong CC, Robertson AW, He K, Lee GD, Yoon E, Allen CS, Kirkland AI, Warner JH (2015) Thermally Induced Dynamics of Dislocations in Graphene at Atomic Resolution. Acs Nano 9 (10):10066-10075
56. N. Mironova-Ulmane AK, I. Steins, J. Grabis, I. Sildos, M. Pärs (2007) Raman scattering in nanosized nickel oxide NiO. Journal of Physics: Conference Series 93:012039
57. Murphy H, Papakonstantinou P, Okpalugo TIT (2006) Raman study of multiwalled carbon nanotubes functionalized with oxygen groups. Journal of Vacuum Science & Technology B 24 (2):715-720
58. R. E. Dietz GIP, A. E. Meixner (1971) Infrared Absorption and Raman Scattering by Two-Magnon Processes in NiO. Physical Review B 4:2302-2310
59. Castillejos E, Bachiller-Baeza B, Perez-Cadenas M, Gallegos-Suarez E, Rodriguez-Ramos I, Guerrero-Ruiz A, Tamargo-Martinez K, Martinez-Alonso A, Tascon JMD (2012) Structural and surface modifications of carbon nanotubes when submitted to high temperature annealing treatments. Journal of Alloys and Compounds 536:S460-S463. doi:10.1016/j.jallcom.2011.11.007
60. Sahoo RK, Daramalla V, Jacob C (2012) Multiwall and bamboo-like carbon nanotube growth by CVD using a semimetal as a catalyst. Mater Sci Eng B-Adv 177 (1):79-85
61. Zhong GF, Xie RS, Yang JW, Robertson J (2014) Single-step CVD growth of high-density carbon nanotube forests on metallic Ti coatings through catalyst engineering. Carbon 67:680-687
62. Hoecker C, Smail F, Bajada M, Pick M, Boies A (2016) Catalyst nanoparticle growth dynamics and their influence on product morphology in a CVD process for continuous carbon nanotube synthesis. Carbon 96:116-124
63. Zhao J, Zhang Y, Su Y, Huang X, Wei L, Kong ES-W, Zhang Y (2012) Structural improvement of CVD multi-walled carbon nanotubes by a rapid annealing process. Diamond and Related Materials 25:24-28. doi:10.1016/j.diamond.2012.01.029

Conflicts of interest

The authors declare that there are no conflicts of interest which could potentially influence the submitted work.